JGR Biogeosciences

RESEARCH ARTICLE
10.1029/2019JG005230

Modeling Holocene Peatland Carbon Accumulation in North America

Qianlai Zhuang[1,2], Sirui Wang[1], Bailu Zhao[1], Filipe Aires[3,4,5], Catherine Prigent[3,4,5], Zicheng Yu[6,7], Jason K. Keller[8], and Scott Bridgham[9]

[1]Department of Earth, Atmospheric, and Planetary Sciences, Purdue University, West Lafayette, IN, USA, [2]Department of Agronomy, Purdue University, West Lafayette, IN, USA, [3]LERMA/Observatoire de Paris, UPMC, CNRS, Paris, France, [4]Columbia Water Center, Columbia University, NY, New York, USA, [5]Estellus, Paris, France, [6]Department of Earth and Environmental Sciences, Lehigh University, Bethlehem, PA, USA, [7]Institute for Mire and Peat Research, School of Geographical Sciences, Northeast Normal University, Changchun, China, [8]Schmid College of Science and Technology, Chapman College, Orange, CA, USA, [9]Institute of Ecology & Evolution, University of Oregon, Eugene, OR, USA

Abstract Peatlands are a large carbon reservoir. Yet the quantification of their carbon stock still has a large uncertainty due to lacking observational data and well-tested peatland biogeochemistry models. Here, a process-based peatland model was calibrated using long-term peat carbon accumulation data at multiple sites in North America. The model was then applied to quantify the peat carbon accumulation rates and stocks within North America over the last 12,000 years. We estimated that 85–174 Pg carbon was accumulated in North American peatlands over the study period including 0.37–0.76 Pg carbon in subtropical peatlands. During the period from 10,000 to 8,000 years ago, the warmer and wetter conditions might have played an important role in stimulating peat carbon accumulation by enhancing plant photosynthesis. Enhanced peat decomposition due to warming slowed the carbon accumulation through the rest of the Holocene. While recent modeling studies indicate that the northern peatlands will continue to act as a carbon sink in this century, our studies suggest that future enhanced peat decomposition accompanied by peatland areal changes induced by permafrost degradation and other disturbances shall confound the sink and source analysis.

Key Points:
- A peatland biogeochemistry model was parameterized and tested using long-term peat carbon accumulation rate data
- The model estimated that 85–174 Pg C was accumulated in North American peatlands during the last 12,000 years
- During the Holocene Thermal Maximum, the warmer and wetter conditions might have resulted in the carbon accumulation peak by enhancing plant photosynthesis in the region

Correspondence to:
Q. Zhuang,
qzhuang@purdue.edu

Citation:
Zhuang, Q., Wang, S., Zhao, B., Aires, F., Prigent, C., Yu, Z., et al. (2020). Modeling Holocene peatland carbon accumulation in North America. *Journal of Geophysical Research: Biogeosciences*, *125*, e2019JG005230. https://doi.org/10.1029/2019JG005230

Received 29 APR 2019
Accepted 26 OCT 2020
Accepted article online 9 NOV 2020

Author Contributions:
Conceptualization: Qianlai Zhuang
Data curation: Bailu Zhao, Filipe Aires, Catherine Prigent, Zicheng Yu, Jason K. Keller, Scott Bridgham
Formal analysis: Qianlai Zhuang, Sirui Wang
Funding acquisition: Qianlai Zhuang
Investigation: Qianlai Zhuang, Sirui Wang, Bailu Zhao, Filipe Aires, Catherine Prigent, Zicheng Yu
Methodology: Qianlai Zhuang, Sirui Wang
Project administration: Qianlai Zhuang
Resources: Filipe Aires, Catherine Prigent
Supervision: Qianlai Zhuang
Validation: Qianlai Zhuang, Sirui Wang, Filipe Aires, Catherine Prigent, Zicheng Yu, Jason K. Keller, Scott Bridgham
(continued)

1. Introduction

Among all terrestrial ecosystems, peatlands form the largest reservoir of soil organic carbon (SOC). Global peatlands occupy approximately 3% (4×10^6 km^2) of the global land area but sequester 400–600 Pg C (1 Pg C = 10^{15} g C) (Clymo, 1998; Gorham, 1991, 1995; Maltby & Immirzi, 1993; Yu et al., 2010). Peatlands have accumulated carbon during the past several thousand years mainly because waterlogged soils decrease their carbon decomposition dominated by anaerobic respiration (Gorham et al., 2012; Jones & Yu, 2010; MacDonald et al., 2006; Turunen et al., 2002). As a result, northern peatlands account for 85–89% of the global peatland SOC stocks (Harden et al., 1992; Kivinen & Pakarinen, 1981). In contrast, tropical and subtropical peatlands only contain 11–15% of the global peatlands SOC (Page et al., 2004, 2011).

Northern peatlands are largely located in the boreal zone of Canada, Russia, Alaska, and Fennoscandian countries (Lappalainen, 1996; Turunen et al., 2002) and have acted as a long-term carbon dioxide (CO_2) sink and methane (CH_4) source during the Holocene period (Bridgham et al., 2006; Jones & Yu, 2010). Recent warming has been projected to intensify in the 21st century, particularly in northern high latitudes (IPCC, 2014), which will change the balance between peat SOC production and decomposition in the future (Frolking et al., 2011; McGuire et al., 2009; Turunen et al., 2002). Recent studies have focused on the mechanism of the responses of peatland carbon accumulation to climate change in the northern high-latitude regions using long-term carbon dating and modeling approaches (Charman et al., 2013; Christensen & Christensen, 2007; Davidson & Janssens, 2006; Dorrepaal et al., 2009; Wang, Zhuang, & Yu, 2016; Wang, Zhuang, Yu, Bridgham, et al., 2016; Yu, 2012; Yu et al., 2009). Warming may lead to greater net primary productivity (NPP) and subsequently enhance peat SOC accumulation, but it may also stimulate soil decomposition and evapotranspiration (Hobbie et al., 2000; Loisel et al., 2012; Yu et al., 2009). In contrast to the view that warming may slow peat SOC accumulation (Dorrepaal et al., 2009), recent studies for the Holocene have indicated that higher temperatures may promote carbon accumulation at millennial

Visualization: Qianlai Zhuang, Sirui Wang, Bailu Zhao
Writing - original draft: Qianlai Zhuang, Sirui Wang
Writing – review & editing: Qianlai Zhuang, Filipe Aires, Catherine Prigent, Zicheng Yu, Jason K. Keller, Scott Bridgham

timescales in northern peatlands (Wang, Zhuang, & Yu, 2016; Wang, Zhuang, Yu, Bridgham, et al., 2016); Jones & Yu, 2010; Loisel et al., 2014). Other climate factors such as the seasonality of photosynthetically active radiation (PAR), the seasonality of temperature, annual precipitation, and growing season length may also play an important role in controlling carbon dynamics in northern peatlands (He et al., 2014; Jones & Yu, 2010; Wang, Zhuang, & Yu, 2016; Wang, Zhuang, Yu, Bridgham, et al., 2016).

Tropical and subtropical peatlands are mainly distributed in Southeast Asia (~56%, Page et al., 2004, 2011) and South and Central America (~23%, Lähteenoja, Ruokolainen, Schulman, & Alvarez, 2009; Lähteenoja, Ruokolainen, Schulman, & Oinonen, 2009). They are largely restricted to poorly drained coastal regions and inland fluvial plains (Gore, 1983; Lähteenoja & Page, 2011; Maltby & Immirzi, 1993). High evapotranspiration rates resulting from warm air temperatures could dry waterlogged areas, warm peat surface temperature, and increase carbon decomposition, limiting the formation of peatlands in tropical and subtropical regions (Chapin et al., 2002; Davidson et al., 2000; Gore, 1983; Trumbore et al., 1996). Recent research suggests that the prevailing climate along with the autogenic processes of peatlands could be important factors affecting tropical peat formation in the Amazon basin. Specifically, Wang et al. (2018) suggested that warming accelerates peat SOC loss, while increasing precipitation stimulates peat SOC accumulation at millennial timescales. Therefore, under warmer and presumably wetter conditions over the 21st century, tropical peatlands are likely to switch from a carbon sink to a *source*. Further, SOC accumulation could also be largely controlled by nonclimate factors such as the transition from minerotrophic to ombrotrophic conditions and the active lateral migration of rivers (Lähteenoja et al., 2012; Lähteenoja & Page, 2011). The largest subtropical wetlands in the United States are the Everglades. These peatlands have their unique geological and hydrological processes and nutrient conditions that led to their development. In comparison to high-latitude peats, these subtropical peats tend to have lower carbohydrate and greater aromatic content, creating a reduced oxidation state and resulting in recalcitrance, allowing peat to persist despite warm temperatures (Hodgkins et al., 2018).

Studies have been conducted to advance the understanding of peat carbon dynamics resulting from climate and geological factors for global peatlands (Kelly et al., 2017; Lähteenoja et al., 2009, 2012; Roucoux et al., 2013; Roulet et al., 2007; Swindles et al., 2014; Turunen et al., 2002; Yu et al., 2009). However, the interaction between peat carbon accumulation and climate change still remains difficult to assess (Loisel et al., 2012, 2014). Two main reasons are as follows: (1) The understanding of the mechanism of peatland responses to climate change is limited (Belyea, 2009; Frolking et al., 2011; Loisel et al., 2014), and (2) there are data gaps and large uncertainties in peat SOC measurements (Yu, 2012). While a number of recent modeling studies have focused on peatland carbon dynamics (e.g., Bona et al., 2020; Chaudhary et al., 2020; Frolking et al., 2010; Kleinen et al., 2012; Qiu et al., 2020; Quillet et al., 2013; Spahni et al., 2013), the peat basal data and carbon stock and flux data obtained in recent years in North America have not been adequately used to parameterize and test process-based peatland biogeochemistry models.

A peatland Terrestrial Ecosystem Model (P-TEM) was recently developed by coupling a hydrological module (HM), a soil thermal module (STM), a methane module (MDM), and a carbon and nitrogen module (CNDM) (Wang et al., 2016b). P-TEM has been parameterized and applied to estimate the regional peat carbon accumulation rates and stocks in Alaska (northern peatlands) and in the Amazon basin (tropical peatlands) (Wang, Zhuang, & Yu, 2016; Wang, Zhuang, Yu, Bridgham, et al., 2016; Wang et al., 2018). Here, we further parameterized and evaluated the model using long-term peat accumulation rate data at multiple sites in Alaska, Canada, the northern conterminous United States, and the Florida Everglades. The model was then applied to simulating the peat SOC accumulation in the past 12,000 years and quantifying the current peat SOC stocks in North America. We acknowledge that this study has not explicitly modeled peatland dynamics but is a first step toward more detailed peatland C modeling for the region.

2. Methods

2.1. Model Framework

2.1.1. Net Ecosystem Production

The peat SOC accumulation rate in the model is equal to the net ecosystem production (NEP), determined by NPP and aerobic and anaerobic respiration (Wang, Zhuang, Yu, Bridgham, et al., 2016; Zhuang et al., 2003). NEP for the peatland ecosystem is calculated at a monthly step:

$$\mathrm{NEP} = \mathrm{NPP} - R_H - R_{CH_4} - R_{CWM} - R_{CM} - R_{COM} \quad (1)$$

NPP is the monthly net primary production. R_H is the monthly aerobic respiration related to the variability of the water table depth, soil moisture, soil temperature, and soil organic C. R_{CH_4} is the monthly methane emission after methane oxidation. R_{CWM} represents the CO_2 emission due to methane oxidation (Zhuang et al., 2015). R_{CM} represents the CO_2 release related to the methanogenesis (Tang et al., 2010). R_{CCOM} represents the CO_2 release from other anaerobic processes (e.g., fermentation and terminal electron acceptor reduction; Keller & Bridgham, 2007). We assume that R_{com}/R_{CH4} is equal to 5.

2.1.2. Net Primary Production

Gross primary production (GPP; see Raich et al., 1991 for details) is defined as the total assimilation of CO_2 by plants, excluding photorespiration. GPP is modeled as a function of PAR, atmospheric CO_2 concentrations, moisture availability, mean air temperature, the relative photosynthetic capacity of the vegetation, and nitrogen availability:

$$\mathrm{GPP} = (C_{max}) \frac{PAR}{k_i + PAR} \frac{C_i}{k_c + C_i} f(PHENOLOGY)\, f(FOLIAGE)\, f(T)\, f(NA) \quad (2)$$

where C_{max} is the monthly maximum rate of C assimilation by the entire plant canopy under optimal environmental conditions (g m^{-2} $month^{-1}$), PAR is photosynthetically active radiation at canopy level (J cm^{-2} day^{-1}), k_i is the irradiance at which C assimilation proceeds at one half of its maximum rate, C_i is the concentration of CO_2 inside leaves (ml L^{-1}), and k_c is the internal CO_2 concentration at which C assimilation proceeds at one half of its maximum rate. $f(PHENOLOGY)$ is monthly leaf area relative to leaf area during the month of maximum leaf area and depends on monthly estimated evapotranspiration (Raich et al., 1991). $f(FOLIAGE)$ is a scaling function that ranges from 0.0 to 1.0 and represents the ratio of canopy leaf biomass relative to maximum leaf biomass. T is monthly air temperature, and NA is nitrogen availability. The function $f(NA)$ models the limiting effects of plant nitrogen status on GPP.

Plant autotrophic respiration (R_A; see Raich et al., 1991 for details) is the total respiration (excluding photorespiration), including all CO_2 production from the various processes of plant maintenance, nutrient uptake, and biomass construction. R_A is the sum of maintenance respiration (R_m) and growth respiration (R_g):

$$R_A = R_m + R_g \quad (3)$$

The maintenance respiration is modeled as a direct function of plant biomass (C_V). We assume that rising temperatures increase maintenance respiration logarithmically with a Q_{10} of 2 over all temperatures:

$$R_m = K_r(C_V)e^{0.0693T} \quad (4)$$

where K_r is the plant respiration of per unit of biomass carbon at 0°C (g g^{-1} $month^{-1}$) and T is the mean monthly air temperature (°C). Growth or construction respiration R_{gt} is estimated to be 20% of the difference between GPP_t and R_{mt}:

$$\mathrm{NPP'_t} = \mathrm{GPP_t} - R_{mt} \quad (5)$$

$$R_{gt} = 0.2\mathrm{NPP'_t} \quad (6)$$

where NPP_t' is the potential net primary production assuming that the conversion efficiency of photosynthate to biomass is 100% and t refers to the monthly time step.

Net primary production (NPP_t) is the difference between GPP_t and autotrophic respiration (R_{At}):

$$\mathrm{NPP_t} = \mathrm{GPP_t} - R_{At} \quad (7)$$

2.1.3. Aerobic Respiration Related to Water Table Depth

SOC aerobic respiration (R_H) is related to the variability of water table depth:

$$R_H = K_d C_{s1} f(M_V) e^{0.069 H_T} \frac{WTD}{LWD} \quad (8)$$

where M_V represents the mean monthly soil water content (percentage of saturation) in the peat unsaturated zone above the water table depth (WTD). K_d is a decomposition coefficient constant. H_T is the mean monthly peat temperature above the lowest water table depth (LWD, a fixed parameter; the soil below is saturated: Granberg et al., 1999). Here LWD is the deepest water table depth at the site within a number of years, which is specified based on observational data or estimated during parameterization, while WTD varies daily. The SOC between LWD and soil surface (C_{s1}) in the transient simulation is obtained after a 2000-year equilibrium run.

2.1.4. R_{CH_4}, R_{CWM}, R_{CM}, and R_{COM}

R_{CH_4} represents the monthly methane emission after methane oxidation (see Zhuang et al. (2004) for details):

$$R_{CH_4} = M_P - M_O \quad (9)$$

where M_P is the monthly methane production via methanogenesis and M_O is the monthly methane oxidation.

M_P is modeled as an anaerobic process that occurs in the saturated zone of the soil profile. It is calculated as the integration of the hourly methanogenesis ($M_P(z,t)$) at each 1-cm layer:

$$M_P = \int_{t=1}^{24\times 30} \int_{z=1}^{100} M_P(z,t)\mathrm{d}t\mathrm{d}z \quad (10)$$

where

$$M_P(z,t) = M_{G0} f(S_{OM}(z,t))\, f(M_{ST}(z,t))\, f(pH(z,t))\, f(R_X(z,t)) \quad (11)$$

M_{G0} is the ecosystem-specific maximum potential methane production rate. $f(S_{OM}(z,t))$ is a multiplier that enhances methanogenesis with increasing methanogenic substrate availability, which is a function of net primary production of the overlying vegetation. $f(M_{ST}(z,t))$ is a multiplier that enhances methanogenesis with increasing soil temperatures. $f(pH(z,t))$ is a multiplier that diminishes methanogenesis if the soil-water pH is not optimal (i.e., pH = 7.5). $f(R_X(z,t))$ is a multiplier that describes the effects of the availability of electron acceptors which is related to redox potential on methanogenesis.

M_O is modeled as the integration of hourly methane oxidation rate ($M_O(z,t)$) at each 1-cm soil layer:

$$M_O = \int_{t=1}^{24\times 30} \int_{z=1}^{100} M_O(z,t)\mathrm{d}t\mathrm{d}z \quad (12)$$

where

$$M_O(z,t) = O_{MAX} f(C_M(z,t)) f(T_{SOIL}(z,t)) f(E_{SM}(z,t)) f(R_{OX}(z,t)) \quad (13)$$

O_{MAX} is the ecosystem-specific maximum oxidation coefficient; $f(C_M(z,t))$ is a multiplier that enhances methanotrophy with increasing soil methane concentrations; $f(T_{SOIL}(z,t))$ is a multiplier that enhances methanotrophy with increasing soil temperatures; $f(E_{SM}(z,t))$ is a multiplier that diminishes methanotrophy if the soil moisture is not at an optimum level. $f(R_{OX}(z,t))$ is a multiplier that enhances methanotrophy as redox potentials increase.

2.2. Model Parameterization

Key parameters of the individual modules including HM, STM, and MDM have been parameterized in our previous studies of northern peatlands and tropical peatlands (see Wang, Zhuang, Yu, Bridgham, et al., 2016, 2018 for details). Here, we readjusted those key parameters (Table 1) based on the annual C fluxes and pools at multiple sites in North America. We first conducted the initial Monte Carlo simulations to get the proper prior range of the parameter space for peatland ecosystems based on the original parameter space obtained from our previous studies. Annual C fluxes and pools taken from two sites in Alaska

Table 1
Description of the Model Parameters and Their Final Values After Optimization via (1) Initial Monte Carlo Simulations and (2) Second Step Monte Carlo Simulations and Bayesian Inference

Variables	Description	Unit	Latitude 60–72°	Latitude 49–60°	Latitude 45–49°	Latitude 40–45°	Subtropical
C_V	Initial organic C stocks in vegetation	g m^{-2}	633.45 ± 108	633.45 ± 108	633.45 ± 108	633.45 ± 108	13671.05 ± 1,291
C_S	Initial organic C stocks in soil	g m^{-2}	11859.75 ± 1,542	11859.75 ± 1,542	11859.75 ± 1,542	11859.75 ± 1,542	12204.04 ± 1,636
C_{max}	Maximum rate of C assimilation through photosynthesis	g m^{-2} $month^{-1}$	586.35 ± 54	1260.99 ± 121	912.78 ± 78	1300.99 ± 153	859.42 ± 65
CFALL	Proportion of vegetation C loss as litterfall	g g^{-1} $month^{-1}$	0.036 ± 0.009	0.028 ± 0.007	0.03 ± 0.008	0.038 ± 0.009	0.031 ± 0.008
C_{VLmax}	Maximum canopy leaf C	g m^{-2}	124.02 ± 11	129.37 ± 13	128.32 ± 13	126.34 ± 13	454.5 ± 22
K_d	Aerobic heterotrophic respiration at 0°C	2g g^{-1} $month^{-1}$	0.011 ± 0.0005	0.012 ± 0.0005	0.0097 ± 0.0003	0.012 ± 0.0005	0.012 ± 0.0005
T_{min}	Minimum temperature for GPP	°C	− 1.0	− 1.0	− 1.0	0.0	10.0
T_{optmin}	Minimum optimum temperature for GPP	°C	5.5	5.5	14.0	17.0	21.9
T_{optmax}	Maximum optimum temperature for GPP	°C	20.0	20.0	25.0	30.9	32.7
T_{max}	Maximum temperature for GPP	°C	22.0	22.0	30.0	34.0	37.0
D_{moss}	Thickness of moss layer	cm	10.0	10.0	10.0	10.0	10.0
D_{org}	Thickness of organic layer above *LWB*	cm	20.0	20.0	20.0	20.0	20.0
LWB	Lowest water table depth	cm	30.0 ± 5.2	30.0 ± 5.2	30.0 ± 5.2	30.0 ± 5.2	30.0 ± 5.2
P_{tot}	Total porosity of the two layers	%	94, 88	95, 88	95, 83	95, 88	98, 90
S_{min}	Minimum surface soil moisture	cm	25 ± 2	33 ± 2.7	38 ± 3.2	33 ± 2.7	30 ± 2.7
d_{max}	Maximum depth below the peat surface above which the soil moisture starts to decrease linearly	cm	7 ± 3	7 ± 3	8 ± 3	7 ± 3	7 ± 3

Note. The values are the means with 1.96 standard deviation from the posterior distributions for each latitude group after the optimization. T_{min}, T_{optmin}, T_{optmax}, T_{max}, D_{moss}, D_{org}, and P_{tot} were prescribed.

(APEXCON and APEXPER) were used to obtain the prior distribution for northern peatlands during the initial parameterization (Table 2). Annual C fluxes and pools taken from the large Shark River Slough (SRS) basin and the Taylor River/C-111/Florida Bay Basin (TS/Ph) in South Florida were used to obtain the prior distributions for subtropical peatlands in the Great Everglades and other coastal regions (Table 2). A Latin Hypercube Sampler (Iman & Helton, 1988) was applied to draw 5,000 sets of parameters from their uniform distributions. The model was then driven by the climate data (Figure 1) from 1900 to 1990 Common Era (CE). We averaged the simulated monthly C fluxes and pools including aboveground NPP, annual belowground NPP, annual total NPP, aboveground vegetation carbon, belowground vegetation carbon, and total vegetation carbon to annual values and then averaged them from 1900 to 1990 CE. All parameter sets were selected so the simulated annual C fluxes and pools were within the uncertainty ranges of the field measurements (Table 3). The prior distribution of parameters for *Sphagnum* open fen and *Sphagnum* black spruce bog was then merged to represent the prior distribution of parameters for northern peatlands. Similarly, the prior distribution of parameters for sawgrass swamp and mangrove tree island was merged to represent the prior distribution of parameters for subtropical peatlands. These two sets of parameter priors were used to develop parameter posteriors.

Table 2
Description of Sites in Northern Peatlands and Subtropical Peatlands and Variables Used for Parameterizing the Carbon Fluxes and Pools in Core Carbon and Nitrogen Module (CNDM)

Site[a]	Vegetation	Observed variables for CNDM parameterization	References
APEXCON and APEXPER	Moderate rich open fen with sedges (*Carex* sp.), spiked rushes (*Eleocharis* sp.), Sphagnum spp., and brown mosses (e.g., *Drepanocladus aduncus*); Peat plateau bog with black spruce (*Picea mariana*), Sphagnum spp. and feather mosses	Mean annual aboveground and belowground NPP in 2009; Aboveground biomass in 2009	Chivers et al. (2009), Turetsky et al. (2008), Kane et al. (2010), and Churchill (2011)
SRS-3, SRS-4, TS/Ph-3 TS/Ph-6	Fresh water marshes dominated by sawgrass (*Cladium jamaicense*)	Mean annual aboveground and belowground NPP in 2004; Aboveground and belowground biomass in 2004	Ewe et al. (2006), and Castaneda-Moya et al. (2013)
SRS-4, SRS-5, SRS-6 TS/Ph-6, TS/Ph-7, TS/Ph-8	Freshwater mangrove forests (*C. jamaicense-Eleocharis* sp. and scrub *R. mangle-C. erectus*, *Avicennia germinans* and *L. racemose)*	Mean annual aboveground and below ground NPP in 2004; aboveground and belowground biomass in 2004	Same as above

[a]The Alaskan Peatland Experiment (APEX) site is adjacent to the Bonanza Creek Experimental Forest (BCEF) site, approximately 35 km southwest of Fairbanks, AK. (Hinzman et al., 2006). The large Shark River Slough (SRS) basin discharge is channeled via Shark River. The Taylor River/C-111/Florida Bay Basin (TS/Ph) drains southeast Everglades National Park and is a much smaller basin that drains into a considerably larger estuarine and subtidal area. A ratio of 0.47 was used to convert vegetation biomass to carbon for northern peatlands. Annual NPP of sawgrass and mangrove was converted from biomass to carbon based on plant carbon content: Sawgrass biomass contains 48% carbon and mangrove 44% carbon.

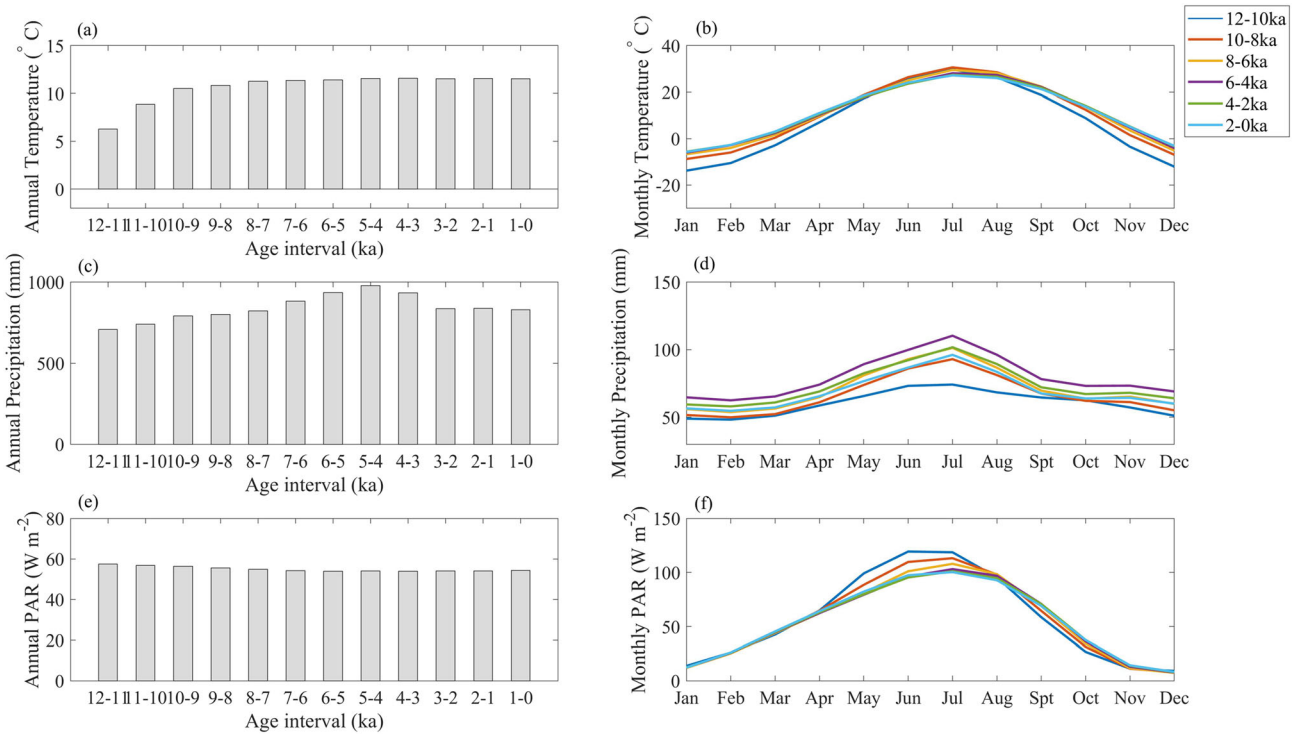

Figure 1. Climate forcing of annual (a) temperature, (c) precipitation, (e) photosynthetically active radiation (PAR) and monthly mean (b) temperature, (d) precipitation, and (f) PAR for North America.

Table 3
Carbon Fluxes and Pools in Northern and Subtropical Peatlands Used for Parameter Optimization of P-TEM

	Sphagnum open fen		Sphagnum black spruce bog		
Annual carbon fluxes or poolsa	Observation	Simulation	Observation	Simulation	References
NPP	445 ± 260	410	433 ± 107	390	
Aboveground vegetation carbon	149–287		423		Turetsky et al. (2008),
Belowground vegetation carbon	347–669		987		Churchill (2011), Moore et al. (2002),
Total vegetation carbon	496–856	800	1,410	1,300	Zhuang et al. (2002),
Litter fall carbon flux	300	333	300	290	Tarnocai et al. (2009),
Methane emission flux	19.5	19.2	9.7	12.8	and Kuhry and Vitt (1996)
	Sawgrass swamp		Mangrove tree island		
	Observation	Simulation	Observation	Simulation	
Aboveground NPP	213±18				Ewe et al. (2006); Castaneda-Moya et al. (2013)
Belowground NPP	213±49				
Total NPP	426±67	416	993	904	
Aboveground vegetation carbon	348±120		2,888		
Belowground vegetation carbon	685±110		1,632		
Total vegetation carbon	1,033±230	984	4,520	4,139	

Note. Values in the columns "Observation" refer to values taken from literature, whereas values in the columns "Simulation" refer to the averaged values from all selected plausible parameter sets after the initial Monte Carlo simulations.
[a]Units for annual net primary production (NPP) and litter fall carbon are g C m^{-2} $year^{-1}$. Units for vegetation carbon are g C m^{-2}. Units for methane emissions are g CH_4 − C m^{-2} yr^{-1}. The simulated total annual methane fluxes were compared with the observations at APEXCON in 2005 and SPRUCE in 2012. The observed aboveground and belowground NPP and observed aboveground and belowground vegetation carbon are the mean values from SRS and TS/Ph sites.

To select the most plausible sets of parameters, a Bayes's framework was applied (see Tang and Zhuang (2009) for details):

$$P(\theta|\mathbf{V}) \propto P(\mathbf{V}|\theta)P(\theta) \tag{14}$$

where $P(\theta|\mathbf{V})$ is the posterior after the Bayesian inference conditioned on the available field measurements $\mathbf{V}$. θ is the matrix of the parameters for adjustment. $\mathbf{V}$ is the difference matrix between the Monte Carlo simulations and the corresponding field measurement. $P(\theta)$ is the prior distribution for peatland ecosystems obtained from the initial Monte Carlo ensemble simulation. $P(\mathbf{V}|\theta)$ is the likelihood function, which is calculated as the function of the difference between Monte Carlo simulations and available field measurement. We again applied the LHS algorithm to draw 1,000 sets of parameters from the prior distributions obtained from the previous Monte Carlo simulations. The observational and field measurement data are peat SOC accumulation rates in Alaska, Canada, north conterminous United States, and South Florida (Table 4) in 500-year bins from their basal ages to 2014 CE. We then averaged the simulated monthly SOC accumulation rates at those sites into 500-year bins and compared them with the field measurement data. We next applied the Sampling Importance Resampling (SIR) technique (Skare et al., 2003) to draw 50 highest plausible parameter sets as the posterior distributions. Finally, we grouped the posterior distributions obtained from different sites into five different groups based on their latitudes. We then averaged the posterior parameter space of each site within the corresponding group (Table 4).

2.3. Regional Simulations and Uncertainty Quantification

Basal ages were calculated by averaging the data of all peatland sites from Loisel et al. (2014) and MacDonald et al. (2006) (see Figure 1 in MacDonald et al. (2006) for basal age distribution of northern peatlands). The averaged basal age for northern peatlands in Canada, Alaska, and northern conterminous United States is 12 ka (1 ka = 1,000 years before present), and the averaged basal age for subtropical peatlands in North America is 4 ka. Northern peatlands were grouped into four subregions by their latitudes (e.g., latitude 40–45°, latitude 45–49°, latitude 49–60°, and latitude 60–72°) based on the peatland distribution map taken from Yu et al. (2010). The peatland map was then downscaled into 0.5° by 0.5° resolution (Figure 2). Regional simulations were conducted within each group by applying the averaged parameter sets from their posterior distributions in the corresponding group (see Table 4 for averaged parameter sets from their

Table 4
Description of Sites in Canada, Alaska, Northern Conterminous United States, and Subtropical Regions in the USA Used for Optimizing the Model Parameters From Their Prior Distributions

Site name[a]	Location	Peatland type	Latitude	Longitude	Basal age (cal yr BP)
		Subtropical region			
02-05-21-5 02-05-21-2	South Florida, USA	Sawgrass swamp, ridge and slough	25°17′N	80°53′W	4,500
98-4-23 00-8-7-1	South Florida, USA	Mangrove tree island	25°17′N	80°53′W	3,000
		Latitude 40–45°			
Caribou Bog	Maine, USA	Bog	45°N	69°W	12,500
Sidney Bog	Maine, USA	Bog	44.39°N	69.79°W	11,000
Petite Bog	Canada	Bog	45.1°N	63.94°W	11,000
		Latitude 45–49°			
FRON-2	Canada	Bog	45.97°N	71.13°W	12,500
South Rhody	Upper Michigan, USA	Bog	46.55°N	86.07°W	10,559
Denbigh	North Dakota, USA	Fen	48.22°N	100.5°W	12,455
MAL-2	Canada	Bog	47.6°N	70.97°W	10,500
		Latitude 49–60°			
Sundance Fen	Canada	Fen	53.58°N	116.75°W	11,000
Patuanak	Canada	Internal Lawn	55.85°N	107.68°W	9,000
Joey Lake	Canada	Bog	55.47°N	98.15°W	8,500
JBL3	Canada	Bog	52.87°N	89.93°W	8,000
Nordan's Pond Bog	Canada	Bog	53.6°N	49.17°W	9,000
Slave Lake Bog	Canada	Bog	55.01°N	114.09°W	10,500
		Latitude 60–72°			
Kenai Gasfield	Alaska, USA	Fen	60.45°N	151.25°W	11,408
Horse Trail Fen	Alaska, USA	Fen	60.42°N	150.9°W	13,000
No Name Creek	Alaska, USA	Fen	60.63°N	151.08°W	11,526
Swanson Fen	Alaska, USA	Fen	60.79°N	150.83°W	14,225

Note. Sites were grouped into different latitude regions.
[a]Sites are selected from studies for various latitudes regions (Booth et al., 2004; Camill et al., 2009; Charman et al., 2013; Charman et al., 2015; Gorham et al., 2003; Jones et al., 2014; Lavoie & Richard, 2000; Loisel et al., 2014; Wang, Zhuang, & Yu, 2016; Wang, Zhuang, Yu, Bridgham, et al., 2016; Yu et al., 2010, 2014).

posterior distribution for each group). The regional peat SOC stocks were estimated based on current peat SOC in per unit area and the corresponding peatland area at each pixel (Figure 2; see Aires et al., 2017 for inundation distribution). The inundation map is assumed to be static over the simulation period (12 ka till 2014 CE) by averaging the annual variations within each grid from 1993 to 2007. The peatland area for each grid is estimated based on the inundation map. A 500-year run was conducted for peatland ecosystem ahead of the basal age using parameters of nonpeatland ecosystems to determine the initial SOC within the upper 1-m mineral soil underlying the peat deposit. The parameters used for the 500-year initial simulation were taken from Wang, Zhuang, and Yu (2016) for northern soils and Wang et al. (2018) for subtropical soils.

We quantified the uncertainty of the total peat SOC stocks in North America due to uncertain parameters. Twenty sets of parameters were randomly drawn from the posterior distributions respectively from each latitude group. Based on the randomly selected parameters, all pixels in the study area were assigned with the same climate forcing data (Figure 1).

3. Results and Discussion

3.1. Site-Level Evaluation

Peat SOC accumulation rates were simulated at multiple sites individually to adjust and evaluate the model performance. In the region of latitude 60–72° that covers Alaska and northern Canada, the simulations at

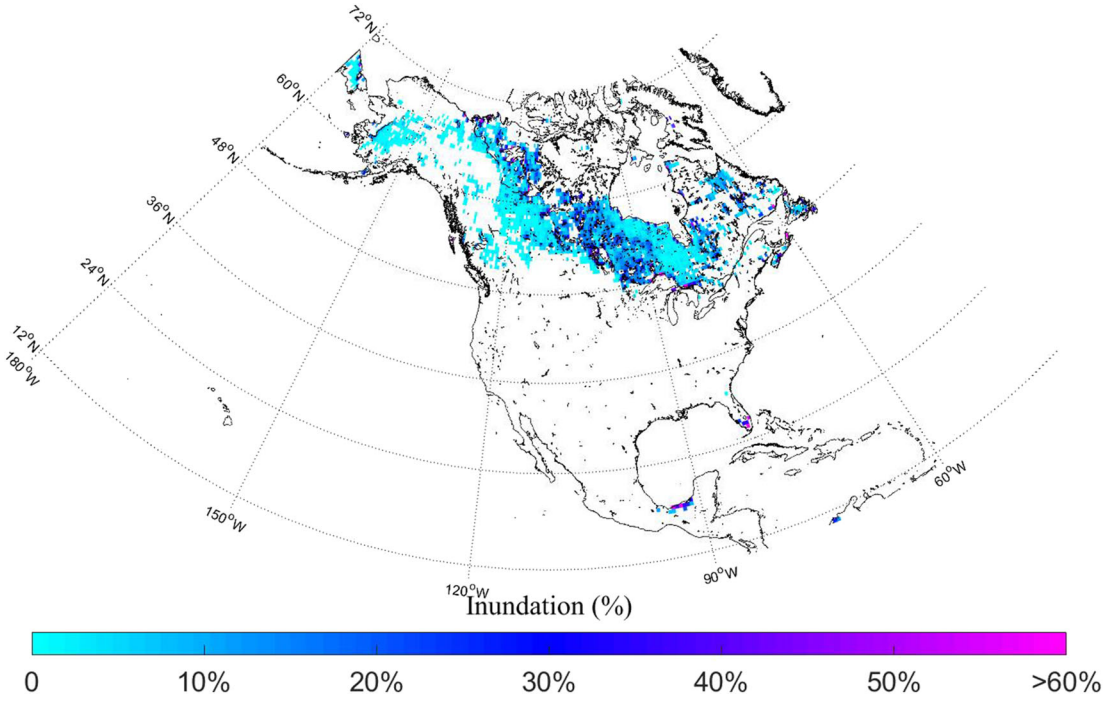

Figure 2. Mean inundation (%) for the peatlands in North America (northern peatlands and subtropical peatlands) at the P-TEM resolution of 0.5° by 0.5° (Aires et al., 2017). Blank areas in the map indicate nonpeatland.

four sites in Alaska in 500-year bins showed a large variation from 15 to 5 ka (Figure 3; see figures in Wang, Zhuang, Yu, Bridgham, et al. (2016) for details). The large peak of SOC accumulation rates at 11–9 ka (during the Holocene Thermal Maximum [HTM]) and the secondary peak at 6–5 ka were captured with the model at No Name Creek and Horse Trail Fen sites. Overall, the simulated trend was consistent with the curves from the observation (except at Swanson Fen). The R^2 coefficient between the simulation and observation was 0.88 for Horse Trail Fen, 0.87 for No Name Creek, 0.38 for Gasfield, and -0.05 for Swanson Fen. The negative correlation at Swanson Fen may result from the time shifted between the simulated accumulation peak in the late HTM and the observed peak in the early HTM (Wang, Zhuang, Yu, Bridgham, et al. 2016).

In the region of latitude 49–60° that covers the main area of Canada, the 500-year bins indicated a largest peak at 9–8 ka at both Nordan's Pond Bog and Slave Lake Bog sites (Figure 4). This time period was consistent with the high SOC accumulation rate peak that occurred during the late HTM at four sites in Alaska. The largest peak at Sundance Fen and Joey Lake Bog sites shifted to 8.5–8 ka, while the peak at Patuanak Bog site shifted to 7.5–7 ka. No peak was observed at JBL3 Bog site. The magnitudes of the largest peaks at the sites in latitude 49–60° were within the range of 55–90 g C m^{-2} $year^{-1}$, comparable to the largest peaks at the sites in latitude 60–72°, indicating a similar long-term peat SOC accumulation pattern in northern peatlands. P-TEM captured the largest peaks at all sites but underestimated the SOC accumulation rates in nonpeak time periods. At Sundance Fen site, the modeled primary peak shifted 1 ka (Figure 4). The observed pattern of SOC accumulation rates also showed a secondary peak of accumulation at 1.5 ka to 2014 CE (0 ka), with the magnitudes varying from 10 to larger than 100 g C m^{-2} $year^{-1}$. P-TEM underestimated the magnitude at Sundance Fen and Patuanak Bog sites while overestimated the magnitude at Joey Lake Bog, JBL3 Bog, Nordan's Pond Bog, and Slave Lake Bog sites. The R^2 coefficient between the simulation and observation was 0.43 for Patuanak Bog, 0.44 for Joey Lake Bog, 0.46 for Sundance Fen, 0.61 for JBL3 Bog, 0.77 for Nordan's Pond Bog, and 0.84 for Slave Lake Bog.

In the regions of latitude 45–49° and latitude 40–45° in the northern conterminous United States, the observed long-term peat SOC accumulation rates at most sites again showed significant peaks at HTM (10–9 ka) and early-to-middle Holocene (9–7.5 ka) (Figures 5 and 6). The magnitudes of the peaks range from 35 to 95 g C m^{-2} $year^{-1}$, comparable to the regions of latitude 49–60° and latitude 60–72°

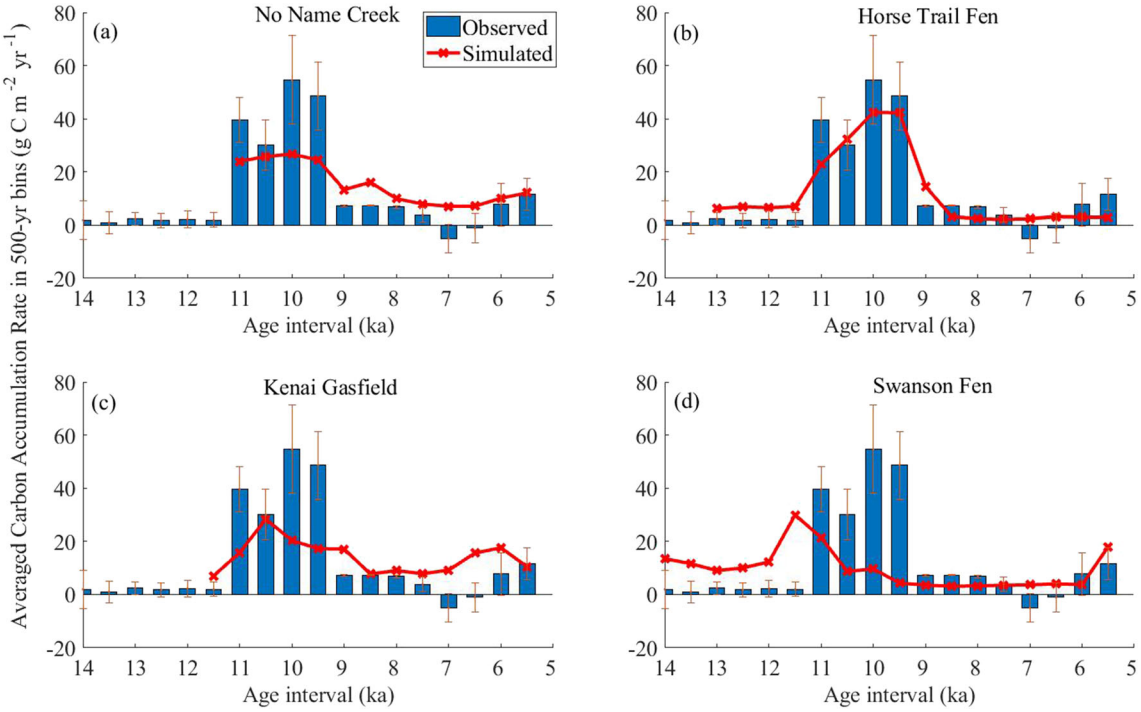

Figure 3. Simulated and observed carbon accumulation rates from 14.5 to 5 ka in 500-year bins in latitude 60–72° for (a) No Name Creek, (b) Horse Trail Fen, (c) Kenai Gasfield, and (d) Swanson Fen (see Figure 4 in Wang, Zhuang, & Yu, 2016).

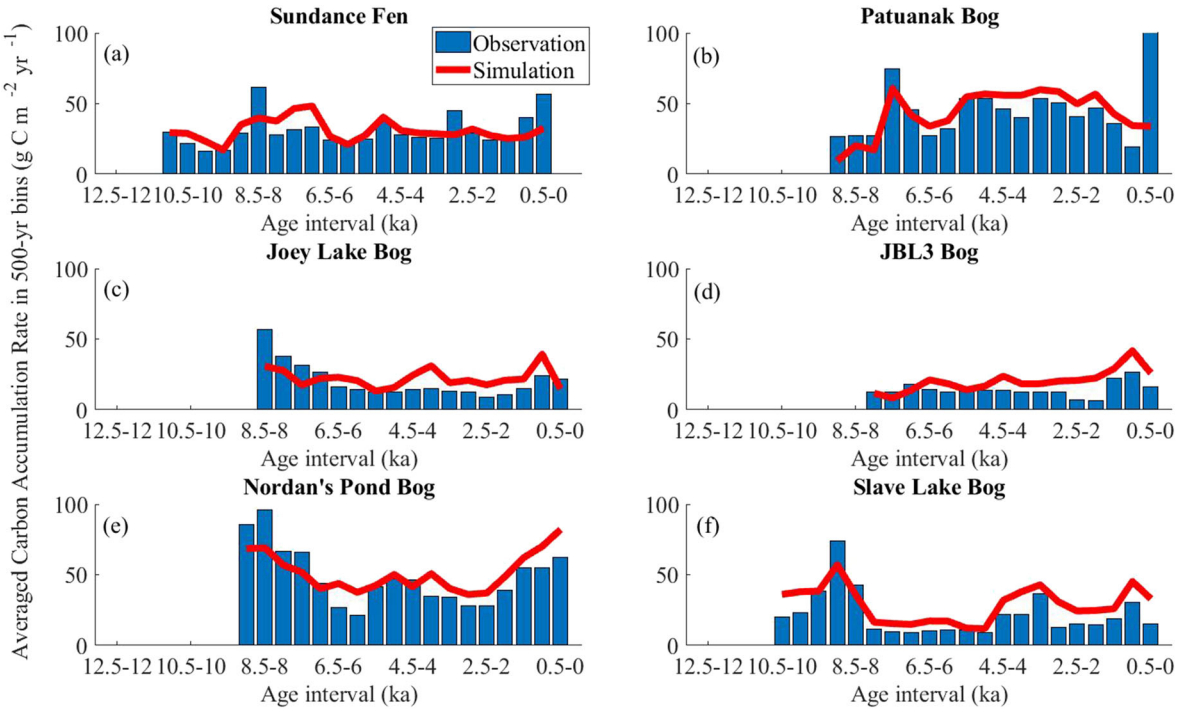

Figure 4. Simulated and observed carbon accumulation rates from 12.5 ka to 2014 CE (0 ka) in 500-year bins in latitude 49–60° for (a) Sundance Fen, (b) Patuanak Bog, (c) Joey Lake Bog, (d) JBL3 Bog, (e) Nordan's Pond Bog, and (f) Slave Lake Bog. Only the comparisons within the time period with available observed data were conducted.

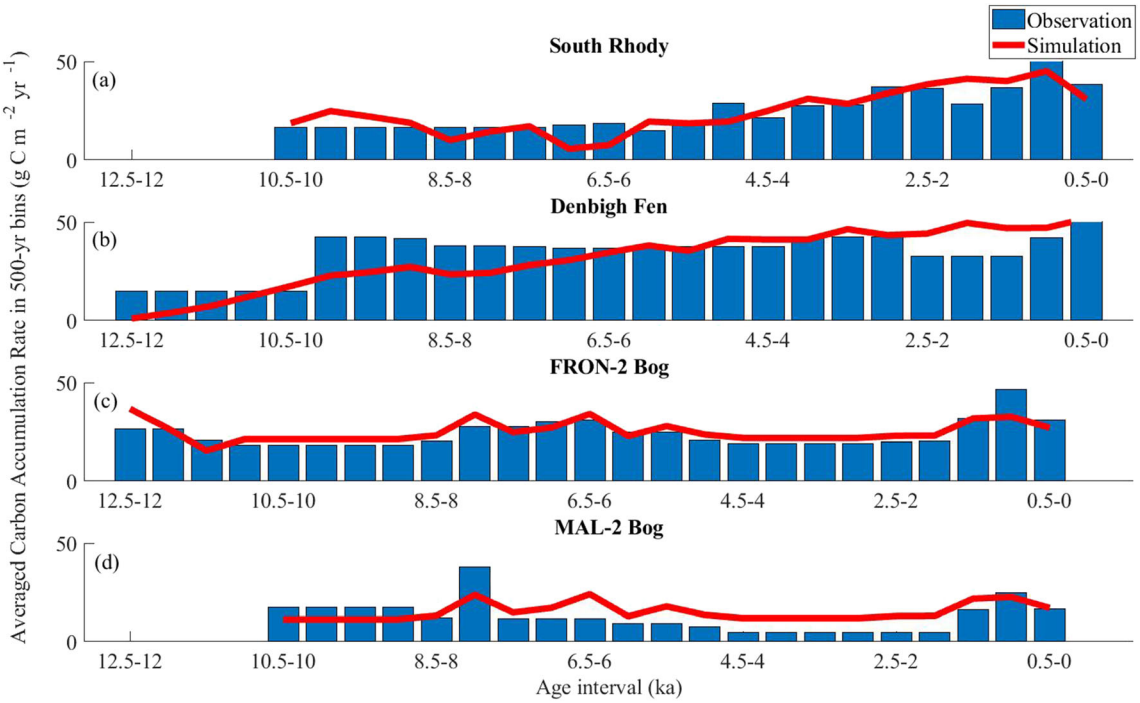

Figure 5. Simulated and observed carbon accumulation rates from 12.5 ka to 2014 CE (0 ka) in 500-year bins in latitude 45–49° for (a) South Rhody, (b) Denbigh Fen, (c) FRON-2 Bog, and (d) MAL-2 Bog. Only the comparisons within the time period with available observed data were conducted.

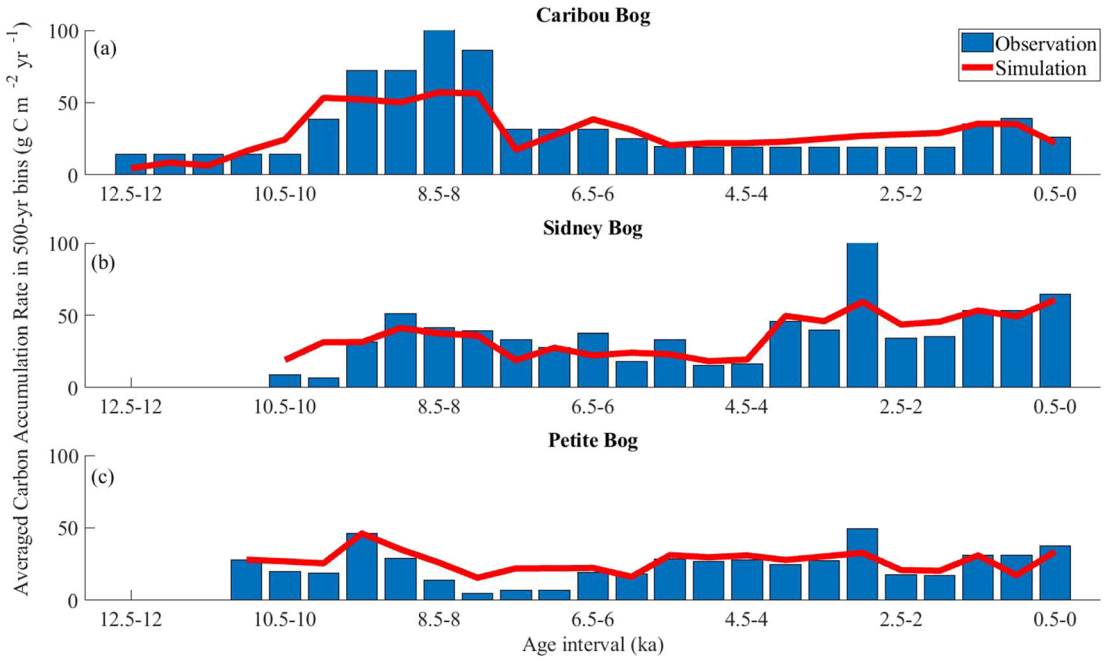

Figure 6. Simulated and observed carbon accumulation rates from 12.5 ka to 2014 CE (0 ka) in 500-year bins in latitude 40–45° for a Caribou Bog, (b) Sidney Bog, and (c) Petite Bog. Only the comparisons within the time period with available observed data were conducted.

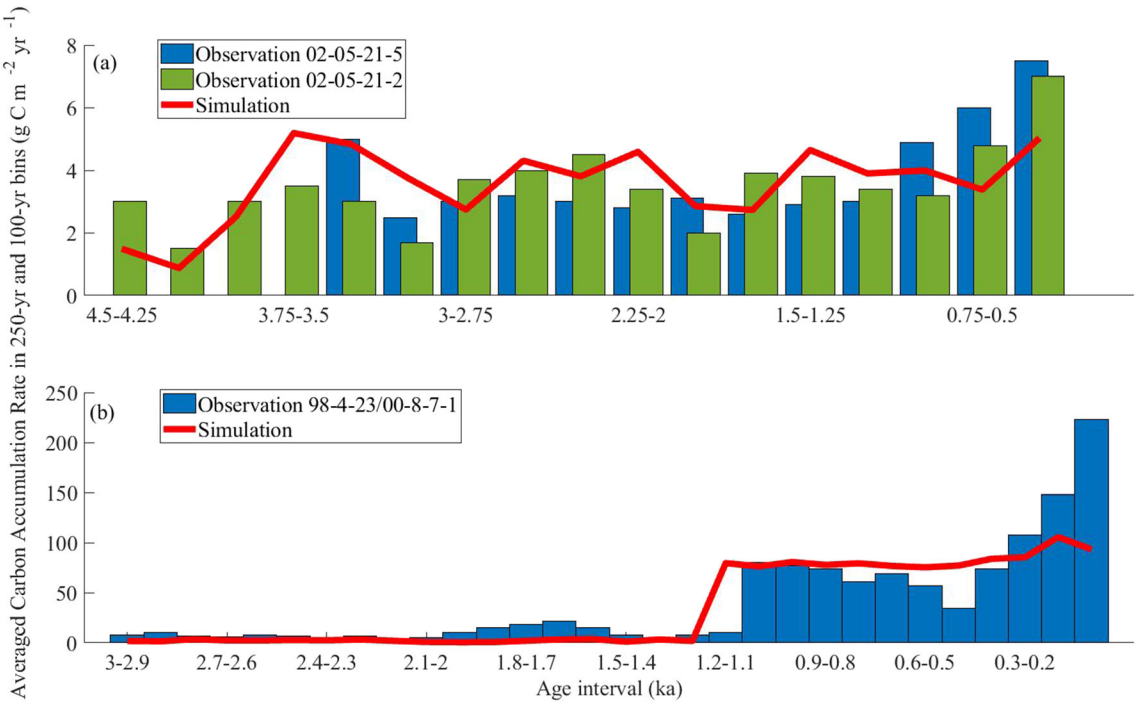

Figure 7. Simulated and observed carbon accumulation rates from 4.5 ka to 2014 CE (0 ka) in 250-year bins in subtropical region for (a) sawgrass and from 3 ka to 2014 CE (0 ka) in 100-year bins for (b) sawgrass and tree island. The transition from sawgrass to tree island was assumed according to the observation (Jones et al., 2014).

(Figures 3 and 4). Caribou Bog site had the most significant increase of accumulation rate, while no obvious peak was observed at South Rhody and FRON-2 Bog sites. The model captured all the primary peaks overall. SOC accumulation peaks at Caribou Bog, Denbigh Fen, and MAL-2 Bog sites were underestimated with the model. The model accurately simulated the peaks at FRON-2 Bog, Sidney Bog, and Petite Bog sites. Similarly, a secondary peak of SOC accumulation rate was observed at all sites at 1 ka to 2014 CE (0 ka). The model reproduced this secondary peak at most of the sites. The R^2 coefficient between the simulation and observation was 0.55 for MAL-2 Bog, 0.70 for Denbigh Fen, 0.74 for FRON-2 Bog, and 0.82 for South Rhody in the region of latitude 45–49°. The R^2 was 0.75 for Petite Bog, 0.78 for Sidney Bog, and 0.84 for Caribou Bog in the region of latitude 40–45°.

In the subtropical region within North America, observed long-term peat SOC showed a large variation between sawgrass (<10 g C m^{-2} $year^{-1}$) peatlands and tree island peatlands (70–200 g C m^{-2} $year^{-1}$) (Figure 7). SOC accumulation rates in 250-year bins showed a similar pattern at 02-05-21-5 and 02-05-21-2 sites with most of the rates below 10 g C m^{-2} $year^{-1}$. Tree island peatlands at the 98-4-23 site had much higher accumulation rates in 100-year bins after 1.1 ka when the transition from sawgrass to tree island was assumed according to the observation (Jones et al., 2014). Peaks at all three sites were captured after 0.5 ka, but nonpeak periods were largely underestimated by the model (Figure 7). The R^2 was 0.45 for site 02-05-21-5, 0.49 for site 02-05-21-2, and 0.80 for site 98–4-23.

3.2. Carbon Accumulation in North America

The peat SOC stock distribution showed a large spatial variation in the region of latitude 60–72° (Figure 8). Peatlands were largely distributed in the west part of the region including Alaska and western Canada. Peatlands in Alaska had a relatively low SOC stocks ranging from 0 to 150 kg C m^{-2} with higher values distributed in central Alaska. Western Canada has much higher SOC up to 400 kg C m^{-2}. In the region of latitude 49–60°, most peatlands had the current SOC between 100 and 300 kg C m^{-2}. Low SOC areas fell within the northern part, south central part, and eastern part of the region with SOC from 100 to 150 kg C m^{-2}. The central part of the region exhibited a higher value with an average of 250 kg C m^{-2}. In the region of latitude

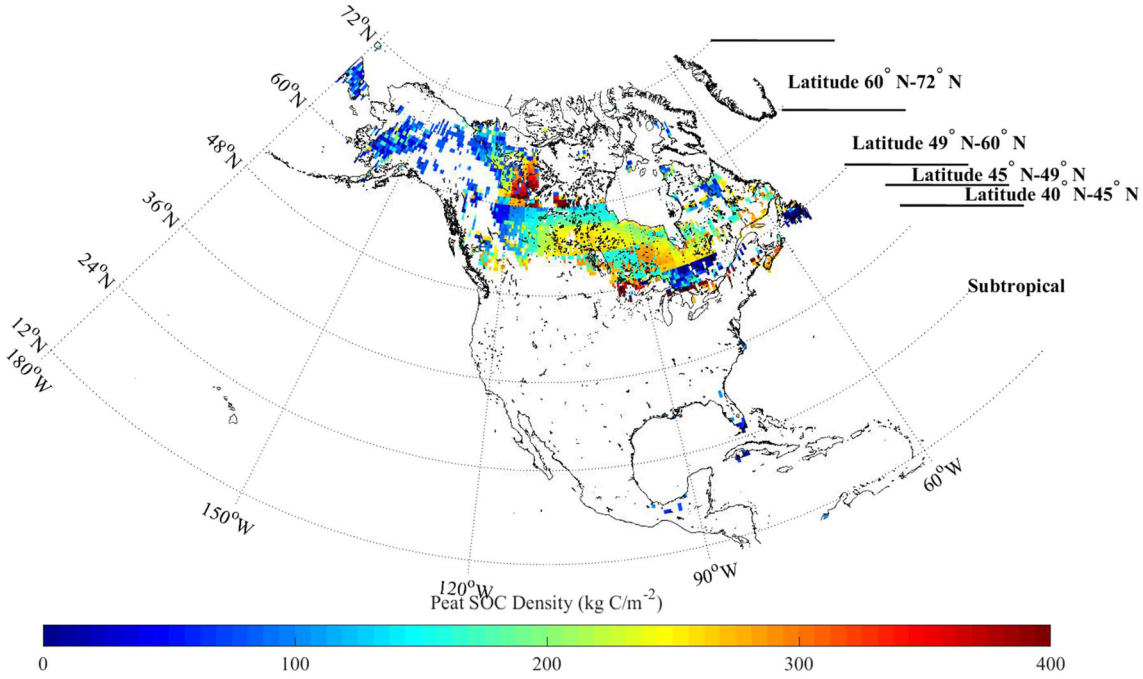

Figure 8. Spatial distribution of the combination of current peat SOC stocks (kg C m^{-2}) in the regions of latitude 60–72°, latitude 49–60°, latitude 45–49°, latitude 40–45°, and subtropics from 12 ka to 2014 CE.

45–49°, a lower SOC was simulated ranging from 0 to 100 kg C m^{-2}. The northern and southern parts of the region had a small amount of SOC, while the central part had a higher value at approximately 130 kg C m^{-2}. A small region in the western part had the highest SOC (>35 kg C m^{-2}). In the region of latitude 40–45°, SOC stocks were moderate (~250 kg C m^{-2}) and had small spatial variations. The peatlands were mainly located in upper Michigan and Maine. In the subtropical region, peatlands were mainly distributed in the Great Everglades and the coastal area of Mexican Gulf. Low SOC was modeled ranging from 0 to 120 kg C m^{-2}. The relatively low stocks in the subtropical regions were presumably due to the much shorter basal age (4 ka) compared with the northern peatlands (12 ka). Peatlands in the whole Northern America showed a large variation and discontinuity, with the highest SOC stocks located within the Hudson Bay Lowland (HBL) in Manitoba, Ontario, and Quebec (Figure 8). The majority of the peatlands are in Canada, Alaska, and northern conterminous United States. Peatlands are not in the HBL, and Northwest Territories of Canada had moderate SOC stocks, while the northern part of the United States and Alaska had lower stocks. The large discontinuity among different simulation regions resulted from implementing different sets of parameters during the regional simulation (Table 1). It is worth noting that the model has not been parameterized for the HBL peatlands, which might have biased our regional estimates given that the HBL peatlands are the largest peatland area in North America (e.g., Helbig et al., 2019; Humphreys et al., 2014; McLaughlin & Webster, 2014; Packalen et al., 2014).

The model simulated the largest peak of peat SOC accumulation rate from 10 to 8 ka (Figure 9a). On average, the simulated SOC accumulation is 17.16 g C m^{-2} $year^{-1}$ from 12 ka to 2014 CE. However, the SOC accumulation rates at 10–8 ka abruptly increased to 40 g C m^{-2} $year^{-1}$, 2 times higher than the average rate during the whole simulation period. These were consistent with the findings of recent studies (Jones & Yu, 2010; Yu et al., 2009), indicating that, during the HTM, the expansion and formation of northern peatlands reached their highest. The simulated climate by CCSM3 (TraCE-21 ka) model showed that the coolest temperature appeared at 15–10 ka (Figures 1a and 1b) in the whole North America (NA). The Arctic region of NA had colder and drier climate before the onset of the HTM (Barber & Finney, 2000; Edwards et al., 2001). It is worth noting that our simulations have not considered the impacts of peatland dynamics including initiation, expansion, shrinkage, and shift from one type to another on carbon dynamics. However, in Alaska and Canada, short-term peatland dynamics (e.g., at decadal time scales) are significant due to thaw-

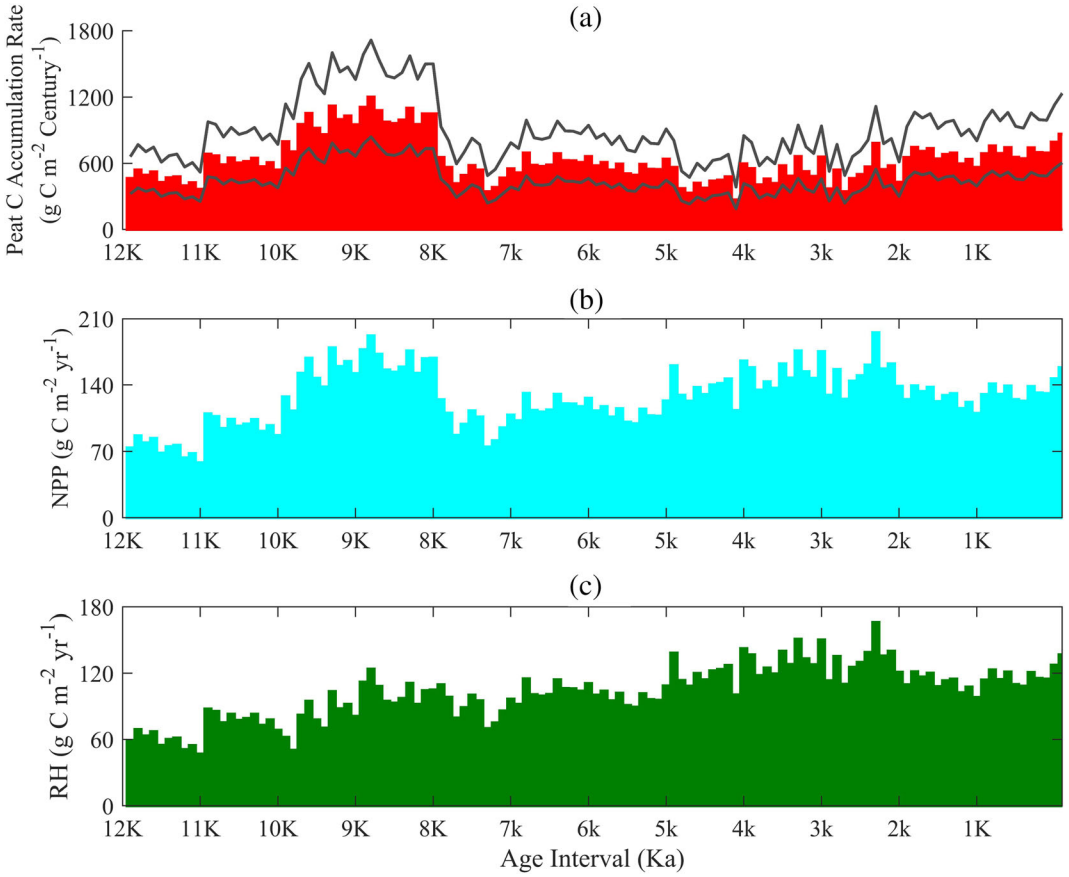

Figure 9. Simulated long-term (a) peat SOC accumulation rates (red bars) with uncertainty ranges (upper and lower black lines); values are accumulated amount over each century, (b) NPP, and (c) heterotrophic respiration (aerobic + anaerobic) of peatlands in North America. Values are annual averages over each century.

ing permafrost and other land morphological changes as documented in Klein et al. (2005), McPartland et al. (2019), and Riordan et al. (2006), which will affect carbon accumulation rates. Indeed, our previous study for Alaska peatlands shows that vegetation distribution has a significant influence on carbon dynamics, even larger than climatic forcing in our simulations (He et al., 2014). Yet we have to admit it is challenging to document the vegetation and peatland dynamics for our whole study spatial and temporal domain given the limited amount of available data. The assumption of static peatland distribution made in this study will no doubt introduce uncertainties in our estimates. Reconstruction of both vegetation and peatland dynamics is needed to evaluate their impacts on carbon accumulation in this region.

The simulated long-term NPP at a yearly step reached its maximum at 10–8 ka, parallel to the peak in the SOC accumulation trend (Figures 9a and 9b). When NPP started increasing at the beginning of the HTM, temperature started rising from 5°C to 10°C (Figure 1a). Meanwhile, annual precipitation during the HTM started increasing from 650 mm and continued until 5 ka to reach its highest level at 1,000 mm (Figures 1c and 1d). Warmer temperature and wetter conditions during the HTM accelerated plant photosynthesis and subsequently increased NPP, as shown by several studies (Kimball et al., 2004; Linderholm, 2006; Tucker et al., 2001). Higher annual precipitation also raised the water table in peatlands and thus allowed more space for anaerobic respiration. While warming continued after the HTM, our model indicated a decrease in SOC accumulation rates accompanied by the continued increase of both aerobic and anaerobic respiration (Figure 9c). NPP also decreased after 8 ka (Figure 9b). The decrease in SOC accumulation could be due to the increased soil organic matter decomposition, as warmer temperatures stimulated soil decomposition. Simulated annual heterotrophic respiration (R_H) followed a pattern similar to the temperature (Figure 1a). Warming also stimulated evapotranspiration and subsequently lowered the water table

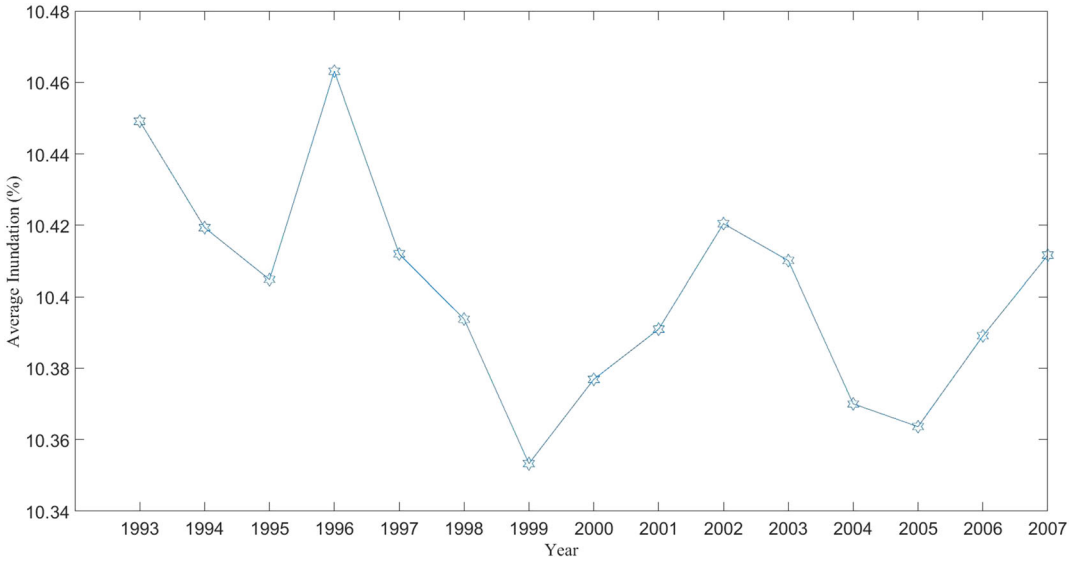

Figure 10. Annual average of inundation fraction of the peatlands in North America from 1993 to 2007.

which had an opposing effect to the higher precipitation. The SOC accumulation rate slightly increased after 3 ka, presumably due to the continued wetter condition after 5 ka (Figure 1a) where NPP might have compensated the increasing R_H caused by warming. Our previous studies indicated that temperature had the most significant effect on peat SOC accumulation rate, followed by the seasonality of net incoming solar radiation (NIRR, Wang, Zhuang, & Yu, 2016; Wang, Zhuang, Yu, Bridgham, et al., 2016). The seasonality of temperature, the interaction of temperature and precipitation, and precipitation alone are all significant causes. As warming continues in the 21st century, the rapid peat SOC accumulation during the HTM under warming and wetter climate might continue to be a larger C sink in this century, as predicted by recent studies (Davidson & Janssens, 2006; Jones & Yu, 2010; Loisel et al., 2012; Spahni et al., 2013; Yu et al., 2009). However, our results suggested that continue warming has positive effects on heterotrophic respiration in northern peatlands as indicated by the simulated long-term R_H (Figure 9c). The future warming effect on soil decomposition might overwhelm its positive effect on plant photosynthesis and could possibly switch the role of the northern peatlands from a long-term carbon sink to a *source*. Moreover, periodic droughts and fire disturbances will also affect peatland dynamics and enhance carbon loss to the atmosphere (e.g., Burd et al., 2020; Swindles et al., 2019). This carbon source estimate is contradicted by the recent modeling studies that suggested that the northern peatlands will continue to act as a carbon sink in this century (Chaudhary et al., 2020; Qiu et al., 2020). While these studies have considered the impacts of peatland areal changes on carbon accumulation, the complex impacts of permafrost degradation and aggradation and other disturbances (e.g., peat fires) on hydrological and peatland dynamics shall be refined. Subsequently, the quantification of the source and sink activities of these peatlands is still elusive.

The peat SOC stocks in each grid pixel at the resolution of 0.5 ° by 0.5 ° were multiplied by the percentage of peatlands from the inundation map (Figure 2). It was then multiplied by the corresponding grid area (56 km by 56 km) to get the total peat SOC stock for North America. Peats were estimated to store a total of 85–174 Pg C (1 Pg C = 10^{15} g C) with a mean of 122 Pg C. The uncertainty range results from the random selection of the parameter sets from their posterior distribution after the model parameterization. Approximately 0.53 Pg C (0.37–0.76 Pg C) is stored in subtropical peatlands, and the majority amount is stored in northern peatlands of North America. Specifically, the northern conterminous United States, Alaska, and Canada account for 0.64%, 0.62%, and 98.74% of the total 121 Pg peat carbon, respectively. Our model was well parameterized and tested for subtropical, temperate, and Alaskan peatlands, but more carbon accumulation and flux data were needed for Canadian peatlands (Tables 3 and 4). This deficiency might have biased our carbon estimates for Canadian peatlands. If we consider the interannual inundation areal variations instead of using average values, the peatlands in North America would store from 84.7 to 85.3 Pg C by assuming that the inundation area changes during our simulation period have the same uncertainty as during 1993–2007 (Figure 10).

In our previous studies on Alaskan peatlands SOC stocks (Wang, Zhuang, & Yu, 2016; Wang, Zhuang, Yu, Bridgham, et al., 2016), vegetation distribution changes reconstructed from fossil pollen data (He et al., 2014) were applied through different time periods over the Holocene to mimic peatland expansion and shrinkage. In this study, we assumed that vegetation changes through time (e.g., peatland area changes) were static during the last 12,000 years. This may oversimplify the complicated variation and evolution of landscape by using modern peatland distribution map as vegetation shifts could happen within hundreds of years (Ager & Brubaker, 1985). In contrast, Qiu et al. (2020) modeled carbon dynamics of northern peatlands by estimating peatland areal changes, highlighting that undisturbed northern peatlands are small but persistent carbon sinks in the future. Similarly, Chaudhary et al. (2020) employed an individual- and patch-based dynamic global vegetation model to quantify long-term carbon accumulation rates in northern peatlands. They found that peatlands in the pan-Arctic continue to act as carbon sinks under future warming scenarios, but rapid global warming could reduce the carbon sink capacity of the northern peatlands in the coming decades. It will be important to compare these estimates to our future simulations for the 21st century, while our current modeling focused on the last 12,000 years.

This study used modern inundation map to quantify carbon stocks within each grid pixel. Specifically, we superimposed the inundation map (Aires et al., 2017) to a peatland map (Yu et al., 2010) to estimate the peatland area, which was used to quantify carbon accumulation for each pixel. Averaging the annual variation of inundation in each grid from 1993 to 2007 to represent the static inundation map over the simulation period also caused uncertainties as inundation data vary from year to year (Figure 10). Using a relatively coarse resolution (56 km by 56 km) for regional model simulation and subsequent carbon stock estimation may also induce a large uncertainty. Additionally, there were uncertainties in estimating peatland basal ages by simply averaging the data from a number of peatland sites that might not be adequate to represent the whole North America. Thus, using the averaged basal age during the regional simulation might also bias our estimates. In summary, while the model was incorporated with sufficient details of peatland processes including plant production and peat decomposition; more detailed basal age data are needed to adequately quantify the peat carbon accumulation at small spatial and short time scales for the region.

4. Conclusions

This study applied a process-based biogeochemistry peatland model to quantify C accumulation rates and C stocks within North America peatlands over the last 12,000 years. The model parameters were optimized by comparing the modeled peat SOC accumulation rates with the long-term observed data at multiple sites in Alaska, Canada, the northern conterminous United States, and the subtropical regions in North America. Consistent with our previous studies on Alaska peatlands and other studies on northern peatlands, our regional simulation captured a primary peak with the highest C accumulation rates during the HTM. Warmer temperature along with wetter conditions might have been the controlling factors to stimulate peat formation by increasing net primary production. Warmer climate decreased the peat accumulation through enhancing heterotrophic respiration and evapotranspiration over the rest of the Holocene. Model simulations indicate that 85–174 Pg C has been accumulated in North American peatlands over the last 12,000 years with 0.37–0.76 Pg C stored in subtropical peatlands, while the rest was mainly stored in Canada. Our study provides an alternative way to quantifying the current peatlands carbon storage by explicitly modeling peatland carbon accumulation rate as a balance between plant productivity and peat decomposition based on existing peatland basal data as well as peatland carbon flux data. Our simulation suggests that, while future warming may stimulate peat plant productivity, this positive effect might not be able to fully compensate the peat carbon loss due to the enhanced peat decomposition, which might switch the northern peatlands from a long-term carbon sink to a *source*. A significant uncertainty of our model estimates is from using a static vegetation and peatland distribution map in our simulation. Future model and data development of peatland dynamics including peatland initiation, expansion, shrinkage, and shifting shall help constrain the uncertainty.

Data Availability Statement

Data access: All data used in this manuscript can be accessed in Purdue University Research Repository (PURR, https://purr.purdue.edu/publications/3531/1).

Acknowledgments

This study is financially supported by a NSF project (1802832), a United States Geological Survey project (G17AC00276), and Department of Energy projects (DE-SC0008092 and DE-SC0007007).

References

Ager, T. A., & Brubaker, L. (1985). Quaternary palynology and vegetational history of Alaska. Pollen Records of Late Quaternary North American Sediments, 353–384.

Aires, F., Miolane, L., Prigent, C., Pham-Duc, B., Fluet-Chouinard, E., Lerner, B., & Papa, F. A. (2017). Global dynamic long-term inundation extent dataset at high spatial resolution derived through downscaling of satellite observations. *Journal of Hydrometeorology*, *18*(5), 1305–1325. https://doi.org/10.1175/JHM-D-16-0155.1

Barber, V. A., & Finney, B. P. (2000). Late Quaternary paleoclimatic reconstructions for interior Alaska based on paleolake-level data and hydrologic models. *Journal of Paleolimnology*, *24*(1), 29–41.

Belyea, L. R. (2009). Nonlinear dynamics of peatlands and potential feedbacks on the climate system. Carbon cycling in northern peatlands, 5-18.

Bona, K. A., Shaw, C., Thompson, D. K., Hararuk, O., Webster, K., Zhang, G., et al. (2020). The Canadian model for peatlands (CaMP): A peatland carbon model of national greenhouse gas reporting. *Ecological Modelling*, *431*, 109164. https://doi.org/10.1016/j.ecolmodel.2020.109164

Booth, R. K., Jackson, S. T., & Gray, C. E. D. (2004). Paleoecology and high-resolution paleohydrology of a kettle peatland in upper Michigan. *Quaternary Research*, *61*, 1–13.

Bridgham, S. D., Megonigal, J. P., Keller, J. K., Bliss, N. B., & Trettin, C. (2006). The carbon balance of North American wetlands. *Wetlands*, *26*(4), 889–916.

Burd, K., Estop-Aragonés, C., Tank, S. E., & Olefeldt, D. (2020). Lability of dissolved organic carbon from boreal peatlands: Interactions between permafrost thaw, wildfire, and season. *Canadian Journal of Soil Science*. https://doi.org/10.1139/cjss-2019-0154

Camill, P., Barry, A., Williams, E., Andreassi, C., Limmer, J., & Solick, D. (2009). Climate-vegetation-fire interactions and their impact on long-term carbon dynamics in a boreal peatland landscape in northern Manitoba, Canada. *Journal of Geophysical Research*, *114*, G04017. https://doi.org/10.1029/2009JG001071

Castaneda-Moya, E., Twilley, R. R., & Rivera-Monroy, V. H. (2013). Allocation of biomass and net primary productivity of mangrove forests along environmental gradients in the Florida coastal Everglades, USA. *Forest Ecology and Management*, *307*, 226–241.

Chapin, F. S., Matson, P. A., & Mooney, H. A. (2002). *Principles of terrestrial ecosystem ecology*. New York: Springer.

Charman, D. J., Amesbury, M. J., Hinchliffe, W., Hughes, P. D., Mallon, G., Blake, W. H., et al. (2015). Drivers of Holocene peatland carbon accumulation across a climate gradient in northeastern North America. *Quaternary Science Reviews*, *121*, 110–119.

Charman, D. J., Beilman, D. W., Blaauw, M., Booth, R. K., Brewer, S., Chambers, F. M., et al. (2013). Climate-related changes in peatland carbon accumulation during the last millennium. *Biogeosciences*, *10*(2), 929–944. https://doi.org/10.5194/bg-10-929-2013

Chaudhary, N., Westermann, S., Lamba, S., Shurpali, N., Sannel, A., Schurgers, G., et al. (2020). Modelling past and future peatland carbon dynamics across the pan-Arctic. *Global Change Biology*, *26*(7), 4119–4133. https://doi.org/10.1111/gcb.15099

Chivers, M. R., Turetsky, M. R., Waddington, J. M., Harden, J. W., & McGuire, A. D. (2009). Effects of experimental water table and temperature manipulations on ecosystem CO_2 fluxes in an Alaskan rich fen. *Ecosystems*, *12*(8), 1329–1342.

Christensen, J. H., & Christensen, O. B. (2007). A summary of the PRUDENCE model projections of changes in European climate by the end of this century. *Climatic Change*, *81*(1), 7–30.

Churchill, A. (2011). *The response of plant community structure and productivity to changes in hydrology in Alaskan boreal peatlands* (Master Thesis). University of Alaska, Fairbanks, AK, USA. 119 pp.

Clymo, R. S. (1998). Sphagnum, the peatland carbon economy, and climate change. In J. W. Bates, N. W. Ashton, J. G. Duckett (Eds.). *Bryology for the 21st century* (pp. 361–368). Maney Publishing Company, Leeds, and the Bryological Society.

Davidson, E. A., & Janssens, I. A. (2006). Temperature sensitivity of soil carbon decomposition and feedbacks to climate change. *Nature*, *440*(7081), 165–173.

Davidson, E. A., Trumbore, S. E., & Amundson, R. (2000). Biogeochemistry: Soil warming and organic carbon content. *Nature*, *408*(6814), 789–790. https://doi.org/10.1038/35048672

Dorrepaal, E., Toet, S., van Logtestijn, R. S., Swart, E., van de Weg, M. J., Callaghan, T. V., & Aerts, R. (2009). Carbon respiration from subsurface peat accelerated by climate warming in the subarctic. *Nature*, *460*(7255), 616–619.

Edwards, M. E., Mock, C. J., Finney, B. P., Barber, V. A., & Bartlein, P. J. (2001). Potential analogues for paleoclimatic variations in eastern interior Alaska during the past 14,000 yr: Atmospheric-circulation controls of regional temperature and moisture responses. *Quaternary Science Reviews*, *20*(1), 189–202.

Ewe, S. M. L., Gaiser, E. E., Childers, D. L., Iwaniec, D., Rivera-Monroy, V. H., & Twilley, R. R. (2006). Spatial and temporal patterns of aboveground net primary productivity (ANPP) along two freshwater-estuarine transects in the Florida coastal Everglades. *Hydrobiologia*, *569*, 459–474.

Frolking, S., Roulet, N. T., Tuittila, E., Bubier, J. L., Quillet, A., Talbot, J., & Richard, P. J. H. (2010). A new model of Holocene peatland net primary production, decomposition, water balance, and peat accumulation. *Earth System Dynamics*, *1*(1), 1–21.

Frolking, S., Talbot, J., Jones, M. C., Treat, C. C., Kauffman, J. B., Tuittila, E. S., & Roulet, N. (2011). Peatlands in the Earth's 21st century climate system. *Environmental Reviews*, *19*(NA), 371–396.

Gore, A. J. P. (Ed) (1983). *Mires: Swamp, bog, fen, and moor*. Amsterdam: Elsevier.

Gorham, E. (1991). Northern peatlands: Role in the carbon cycle and probable responses to climatic warming. *Ecological Applications*, *1*(2), 182–195. https://doi.org/10.2307/1941811

Gorham, E. (1995). The biogeochemistry of northern peatlands and its possible responses to global warming. In G. M. Woodwell & F. T. Mackenzie (Eds.), *Biotic feedbacks in the global climate system: Will the warming feed the warming?* (pp. 169–186). New York: Oxford University Press.

Gorham, E., Janssens, J. A., & Glaser, P. H. (2003). Rates of peat accumulation during the postglacial period in 32 sites from Alaska to Newfoundland, with special emphasis on northern Minnesota. *Canadian Journal of Botany*, *81*(5), 429–438.

Gorham, E., Lehman, C., Dyke, A., Clymo, D., & Janssens, J. (2012). Long-term carbon sequestration in North American peatlands. *Quaternary Science Reviews*, *58*, 77–82.

Granberg, G., Grip, H., Löfvenius, M. O., Sundh, I., Svensson, B. H., & Nilsson, M. (1999). A simple model for simulation of water content, soil frost, and soil temperatures in boreal mixed mires. *Water Resources Research*, *35*(12), 3771–3782.

Harden, J. W., Mark, R. K., Sundquist, E. T., & Stallard, R. F. (1992). Dynamics of soil carbon during deglaciation of the Laurentide ice sheet. *Science*, *258*(5090), 1921–1924. https://doi.org/10.1126/science.258.5090.1921

He, Y., Jones, M. C., Zhuang, Q., Bochicchio, C., Felzer, B. S., Mason, E., & Yu, Z. (2014). Evaluating CO2 and CH 4 dynamics of Alaskan ecosystems during the Holocene Thermal Maximum. *Quaternary Science Reviews*, *86*, 63–77.

Helbig, M., Humphreys, E. R., & Todd, A. (2019). Contrasting temperature sensitivity of CO_2 exchange in Peatlands of the Hudson Bay Lowlands, Canada. *Journal of Geophysical Research: Biogeosciences*, *124*, 2126–2143. https://doi.org/10.1029/2019JG005090

Hinzman, L. D., Viereck, L. A., Adams, P. C., Romanovsky, V. E., & Yoshikawa, K. (2006). Climate and permafrost dynamics of the Alaskan boreal forest. Alaska's Changing Boreal Forest, 39-61.

Hobbie, S. E., Schimel, J. P., Trumbore, S. E., & Randerson, J. R. (2000). Controls over carbon storage and turnover in high-latitude soils. *Global Change Biology*, *6*(S1), 196–210.

Hodgkins, S. B., Richardson, C. J., Dommain, R., Wang, H., Glaser, P. H., Verbeke, B., et al. (2018). Tropical peatland carbon storage linked to global latitudinal trends in peat recalcitrance. *Nature Communications*, *9*, 3640.

Humphreys, E. R., Charron, C., Brown, M., & Jones, R. (2014). Two bogs in the Canadian Hudson Bay Lowlands and a temperate bog reveal similar annual net ecosystem exchange of CO2. *Arctic, Antarctic, and Alpine Research*, *46*, 103–113.

Iman, R. L., & Helton, J. C. (1988). An investigation of uncertainty and sensitivity analysis techniques for computer models. *Risk Analysis*, *8*(1), 71–90. https://doi.org/10.1111/j.1539-6924.1988.tb01155.x

IPCC (2014). Climate Change 2014: Synthesis Report. Contribution of Working Groups I, II and III to the Fifth Assessment Report of the Intergovernmental Panel on Climate Change. In Core Writing Team R. K. Pachauri & L. A. Meyer (Eds.) (pp. 151). Geneva, Switzerland: IPCC.

Jones, M. C., Bernhardt, C. E., & Willard, D. A. (2014). Late Holocene vegetation, climate, and land-use impacts on carbon dynamics in the Florida Everglades. *Quaternary Science Reviews*, *90*, 90–105.

Jones, M. C., & Yu, Z. (2010). Rapid deglacial and early Holocene expansion of peatlands in Alaska. *Proceedings of the National Academy of Sciences*, *107*(16), 7347–7352.

Kane, E. S., Turetsky, M. R., Harden, J. W., McGuire, A. D., & Waddington, J. M. (2010). Seasonal ice and hydrologic controls on dissolved organic carbon and nitrogen concentrations in a boreal-rich fen. *Journal of Geophysical Research*, *115*, G04012. https://doi.org/10.1029/2010JG001366

Keller, J. K., & Bridgham, S. D. (2007). Pathways of anaerobic carbon cycling across an ombrotrophic–minerotrophic peatland gradient. *Limnology and Oceanography*, *52*, 96–107.

Kelly, T. J., Lawson, I. T., Roucoux, K. H., Baker, T. R., Jones, T. D., & Sanderson, N. K. (2017). The vegetation history of an Amazonian domed peatland. *Palaeogeography, Palaeoclimatology, Palaeoecology*, *468*, 129–141. https://doi.org/10.1016/j.palaeo.2016.11.039

Kimball, J. S., McDonald, K. C., Running, S. W., & Frolking, S. E. (2004). Satellite radar remote sensing of seasonal growing seasons for boreal and subalpine evergreen forests. *Remote Sensing of Environment*, *90*(2), 243–258.

Kivinen, E., & Pakarinen, P. (1981). Geographical distribution of peat resources and major peatland complex types in the world. *Annales Academiae Scientarum Fennicae, Series A, Number*, *132*.

Klein, E., Berg, E. E., & Dial, R. (2005). Wetland drying and succession across the Kenai Peninsula Lowlands, south-central Alaska. *Canadian Journal of Forest Research*, *35*(8), 1931–1941. https://doi.org/10.1139/x05-129

Kleinen, T., Brovkin, V., & Schuldt, R. J. (2012). A dynamic model of wetland extent and peat accumulation: Results for the Holocene. *Biogeosciences*, *9*(1), 235–248.

Kuhry, P., & Vitt, D. H. (1996). Fossil carbon/nitrogen ratios as a measure of peat decomposition. *Ecology*, *77*(1), 271–275.

Lähteenoja, O., & Page, S. (2011). High diversity of tropical peatland ecosystem types in the Pastaza-Marañón basin, Peruvian Amazonia. *Journal of Geophysical Research*, *116*, G02025. https://doi.org/10.1029/2010JG001508

Lähteenoja, O., Reátegui, Y. R., Räsänen, M., Torres, D. D. C., Oinonen, M., & Page, S. (2012). The large Amazonian peatland carbon sink in the subsiding Pastaza-Marañón foreland basin, Peru. *Global Change Biology*, *18*(1), 164–178. https://doi.org/10.1111/j.1365-2486.2011.02504.x

Lähteenoja, O., Ruokolainen, K., Schulman, L., & Alvarez, J. (2009). Amazonian floodplains harbour minerotrophic and ombrotrophic peatlands. *Catena*, *79*(2), 140–145. https://doi.org/10.1016/j.catena.2009.06.006

Lähteenoja, O., Ruokolainen, K., Schulman, L., & Oinonen, M. (2009). Amazonian peatlands: An ignored C sink and potential source. *Global Change Biology*, *15*(9), 2311–2320. https://doi.org/10.1111/j.1365-2486.2009.01920.x

Lappalainen, E. (1996). General review on world peatlands and peat resources. In E. Lappalainen (Ed.), *Global peat resources* (pp. 53–56). Jyvaskyla: International Peat Society.

Lavoie, M., & Richard, P. J. H. (2000). Paléoécologie de la tourbière du lac Malbaie, dans le massif des Laurentides (Québec): Évaluation du rôle du climat sur l'accumulation de la tourbe. *Géographie Physique et Quaternaire*, *54*, 169–185.

Linderholm, H. W. (2006). Growing season changes in the last century. *Agricultural and Forest Meteorology*, *137*(1), 1–14.

Loisel, J., Gallego-Sala, A. V., & Yu, Z. (2012). Global-scale pattern of peatland Sphagnum growth driven by photosynthetically active radiation and growing season length. *Biogeosciences*, *9*(7), 2737–2746.

Loisel, J., Yu, Z., Beilman, D. W., Camill, P., Alm, J., Amesbury, M. J., et al. (2014). A database and synthesis of northern peatland soil properties and Holocene carbon and nitrogen accumulation. *The Holocene*, *24*(9), 1028–1042. https://doi.org/10.1177/0959683614538073

MacDonald, G. M., Beilman, D. W., Kremenetski, K. V., Sheng, Y., Smith, L. C., & Velichko, A. A. (2006). Rapid early development of circum-arctic peatlands and atmospheric CH4 and CO2 variations. *Science*, *314*(5797), 285–288. https://doi.org/10.1126/science.1131722

Maltby, E., & Immirzi, P. (1993). Carbon dynamics in peatlands and other wetland soils, regional and global perspectives. *Chemosphere*, *27*, 999–1023.

McGuire, A. D., Anderson, L. G., Christensen, T. R., Dallimore, S., Guo, L., Hayes, D. J., et al. (2009). Sensitivity of the carbon cycle in the Arctic to climate change. *Ecological Monographs*, *79*(4), 523–555. https://doi.org/10.1890/08-2025.1

McLaughlin, J., & Webster, K. (2014). Effects of climate change on peatlands in the far north of Ontario, Canada: A synthesis. *Arctic, Antarctic, and Alpine Research*, *46*(1), 84–102. https://doi.org/10.1657/1938-4246-46.1.84

McPartland, M. Y., Kane, E. S., Falkowski, M. J., Kolka, R., Turetsky, M. R., Palik, B., & Montgomery, R. A. (2019). The response of boreal peatland community composition and NDVI to hydrologic change, warming, and elevated carbon dioxide. *Global Change Biology*, *25*(1), 93–107. https://doi.org/10.1111/gcb.14465

Moore, T. R., Bubier, J. L., Frolking, S. E., Lafleur, P. M., & Roulet, N. T. (2002). Plant biomass and production and CO2 exchange in an ombrotrophic bog. *Journal of Ecology*, *90*(1), 25–36.

Packalen, M. S., Finkelstein, S. A., & McLaughlin, J. W. (2014). Carbon storage and potential methane production in the Hudson Bay Lowlands since mid-Holocene peat initiation. *Nature Communications*, *5*(1), 1–8. https://doi.org/10.1038/ncomms5078

Page, S. E., Rieley, J. O., & Banks, C. J. (2011). Global and regional importance of the tropical peatland carbon pool. *Global Change Biology*, *17*(2), 798–818. https://doi.org/10.1111/j.1365-2486.2010.02279.x

Page, S. E., Wűst, R. A. J., Weiss, D., Rieley, J. O., Shotyk, W., & Limin, S. H. (2004). A record of Late Pleistocene and Holocene carbon accumulation and climate change from an equatorial peat bog (Kalimantan, Indonesia): Implications for past, present and future carbon dynamics. *Journal of Quaternary Science*, *19*(7), 625–635. https://doi.org/10.1002/jqs.884

Qiu, C., Zhu, D., Ciais, P., Guenet, B., & Peng, S. (2020). The role of peatlands in the global carbon cycle for the 21st century. *Global Ecology and Biogeography*, *29*(5), 956–973. https://doi.org/10.1111/geb.13081

Quillet, A., Garneau, M., & Frolking, S. (2013). Sobol' sensitivity analysis of the Holocene Peat Model: What drives carbon accumulation in peatlands? *Journal of Geophysical Research: Biogeosciences*, *118*, 203–214. https://doi.org/10.1029/2012JG002092

Raich, J. W., Rastetter, E. B., Melillo, J. M., Kicklighter, D. W., Steudler, P. A., Peterson, B. J., et al. (1991). Potential net primary productivity in South America: Application of a global model. *Ecological Applications*, *1*(4), 399–429. https://doi.org/10.2307/1941899

Riordan, B., Verbyla, D., & McGuire, A. D. (2006). Shrinking ponds in subarctic Alaska based on 1950–2002 remotely sensed images. *Journal of Geophysical Research*, *111*, G04002. https://doi.org/10.1029/2005JG000150

Roucoux, K. H., Lawson, I. T., Jones, T. D., Baker, T. R., Coronado, E. N. H., Gosling, W. D., & Lähteenoja, O. (2013). Vegetation development in an Amazonian peatland. *Palaeogeography, Palaeoclimatology, Palaeoecology*, *374*, 242–255. https://doi.org/10.1016/j.palaeo.2013.01.023

Roulet, N. T., Lafleur, P. M., Richard, P. J., Moore, T. R., Humphreys, E. R., & Bubier, J. I. L. L. (2007). Contemporary carbon balance and late Holocene carbon accumulation in a northern peatland. *Global Change Biology*, *13*(2), 397–411.

Skare, Ø., Bolviken, E., & Holden, L. (2003). Improved sampling importance resampling and reduced bias importance sampling. *Scandinavian Journal of Statistics*, *30*(4), 719–737. https://doi.org/10.1111/1467-9469.00360

Spahni, R., Joos, F., Stocker, B. D., Steinacher, M., & Yu, Z. C. (2013). Transient simulations of the carbon and nitrogen dynamics in northern peatlands: From the Last Glacial Maximum to the 21st century. *Climate of the Past*, *9*(3), 1287–1308.

Swindles, G., Reczuga, M., Lamentowicz, M., Raby, C. L., Turner, T. E., Charman, D. J., et al. (2014). Ecology of testate amoebae in an Amazonian peatland and development of a transfer function for palaeohydrological reconstruction. *Microbial Ecology*, *68*(2), 284–298. https://doi.org/10.1007/s00248-014-0378-5

Swindles, G. T., Morris, P. J., Mullan, D. J., Payne, R. J., Roland, T. P., Amesbury, M. J., et al. (2019). Widespread drying of European peatlands in recent centuries. *Nature Geoscience*, *12*(11), 922–928. https://doi.org/10.1038/s41561-019-0462-z

Tang, J., & Zhuang, Q. (2009). A global sensitivity analysis and Bayesian inference framework for improving the parameter estimation and prediction of a process-based Terrestrial Ecosystem Model. *Journal of Geophysical Research*, *114*, D15303. https://doi.org/10.1029/2009JD011724

Tang, J., Zhuang, Q., Shannon, R. D., & White, J. R. (2010). Quantifying wetland methane emissions with process-based models of different complexities. *Biogeosciences*, *7*(11), 3817–3837.

Tarnocai, C., Canadell, J. G., Schuur, E. A. G., Kuhry, P., Mazhitova, G., & Zimov, S. (2009). Soil organic carbon pools in the northern circumpolar permafrost region. *Global Biogeochemical Cycles*, *23*, GB2023. https://doi.org/10.1029/2008GB003327

Trumbore, S. E., Chadwick, O. A., & Amundson, R. (1996). Rapid exchange between soil carbon and atmospheric carbon dioxide driven by temperature change. *Science*, *272*, 393–396. https://doi.org/10.1126/science.272.5260.393

Tucker, C. J., Slayback, D. A., Pinzon, J. E., Los, S. O., Myneni, R. B., & Taylor, M. G. (2001). Higher northern latitude normalized difference vegetation index and growing season trends from 1982 to 1999. *International Journal of Biometeorology*, *45*(4), 184–190. https://doi.org/10.1007/s00484-001-0109-8

Turetsky, M. R., Treat, C. C., Waldrop, M. P., Waddington, J. M., Harden, J. W., & McGuire, A. D. (2008). Short-term response of methane fluxes and methanogen activity to water table and soil warming manipulations in an Alaskan peatland. *Journal of Geophysical Research*, *113*, G00A10. https://doi.org/10.1029/2007JG000496

Turunen, J., Tomppo, E., Tolonen, K., & Reinikainen, A. (2002). Estimating carbon accumulation rates of undrained mires in Finland—Application to boreal and subarctic regions. *The Holocene*, *12*(1), 69–80.

Wang, S., Zhuang, Q., Lätheenoja, O., Draper, F. C., & Cadillo-Quiroz, H. (2018). Potential shift from a carbon sink to a source in Amazonian peatlands under a changing climate. *Proceedings of the National Academy of Sciences of the United States of America*, *115*, 12,407–12,412.

Wang, S., Zhuang, Q., & Yu, Z. (2016). Quantifying soil carbon accumulation in Alaskan terrestrial ecosystems during the last 15000 years. *Biogeosciences*, *13*(22), 6305–6319. https://doi.org/10.5194/bg-13-6305-2016

Wang, S., Zhuang, Q., Yu, Z., Bridgham, S., & Keller, J. K. (2016). Quantifying peat carbon accumulation in Alaska using a process-based biogeochemistry model. *Journal of Geophysical Research: Biogeosciences*, *121*, 2172–2185. https://doi.org/10.1002/2016JG003452

Yu, Z., Beilman, D. W., & Jones, M. C. (2009). Sensitivity of northern peatland carbon dynamics to Holocene climate change. Carbon cycling in northern peatlands, 55-69.

Yu, Z., Loisel, J., Brosseau, D. P., Beilman, D. W., & Hunt, S. J. (2010). Global peatland dynamics since the Last Glacial Maximum. *Geophysical Research Letters*, *37*, L13402. https://doi.org/10.1029/2010GL043584

Yu, Z., Vitt, D. H., & Wieder, R. K. (2014). Continental fens in Western Canada as effective carbon sinks during the Holocene. *Holocene*, *24*(9), 1090–1104. https://doi.org/10.1177/0959683614538075

Yu, Z. C. (2012). Northern peatland carbon stocks and dynamics: A review. *Biogeosciences*, *9*(10), 4071–4085.

Zhuang, Q., McGuire, A. D., Melillo, J. M., Clein, J. S., Dargaville, R. J., Kicklighter, D. W., et al. (2003). Carbon cycling in extratropical terrestrial ecosystems of the Northern Hemisphere during the 20th century: A modeling analysis of the influences of soil thermal dynamics. *Tellus B*, *55*(3), 751–776. https://doi.org/10.1034/j.1600-0889.2003.00060.x

Zhuang, Q., McGuire, A. D., O'Neill, K. P., Harden, J. W., Romanovsky, V. E., & Yarie, J. (2002). Modeling soil thermal and carbon dynamics of a fire chronosequence in interior Alaska. *Journal of Geophysical Research*, *107*(D1), 8147. https://doi.org/10.1029/2001JD001244

Zhuang, Q., Melillo, J. M., Kicklighter, D. W., Prinn, R. G., McGuire, A. D., Steudler, P. A., et al. (2004). Methane fluxes between terrestrial ecosystems and the atmosphere at northern high latitudes during the past century: A retrospective analysis with a process-based biogeochemistry model. *Global Biogeochemical Cycles*, *18*, GB3010. https://doi.org/10.1029/2004GB002239

Zhuang, Q., Zhu, X., He, Y., Prigent, C., Melillo, J. M., David McGuire, A., et al. (2015). Influence of changes in wetland inundation extent on net fluxes of carbon dioxide and methane in northern high latitudes from 1993 to 2004. *Environmental Research Letters*, *10*(9), 095009. https://doi.org/10.1088/1748-9326/10/9/095009